

Detecting Generated Images by Fitting Natural Image Distributions

Yonggang Zhang¹ Jun Nie^{2,3} Xinmei Tian³ Mingming Gong^{4,6} Kun Zhang^{5,6} Bo Han^{2†}

¹The Hong Kong University of Science and Technology

²TMLR Group, Hong Kong Baptist University ³University of Science and Technology of China

⁴The University of Melbourne, Australia ⁵Carnegie Mellon University

⁶Mohamed bin Zayed University of Artificial Intelligence

Abstract

The increasing realism of generated images has raised significant concerns about their potential misuse, necessitating robust detection methods. Current approaches mainly rely on training binary classifiers, which depend heavily on the quantity and quality of available generated images. In this work, we propose a novel framework that exploits geometric differences between the data manifolds of natural and generated images. To exploit this difference, we employ a pair of functions engineered to yield consistent outputs for natural images but divergent outputs for generated ones, leveraging the property that their gradients reside in mutually orthogonal subspaces. This design enables a simple yet effective detection method: an image is identified as generated if a transformation along its data manifold induces a significant change in the loss value of a self-supervised model pre-trained on natural images. Further more, to address diminishing manifold disparities in advanced generative models, we leverage normalizing flows to amplify detectable differences by extruding generated images away from the natural image manifold. Extensive experiments demonstrate the efficacy of this method. Code is available at <https://github.com/tmlr-group/ConV>.

1 INTRODUCTION

Recent advances in generative models have revolutionized image generation, making it possible to create highly realistic images (Rombach et al., 2022; Dhariwal and Nichol, 2021; Karras et al., 2019). While these generative models offer impressive capabilities, they also introduce significant risks, including the proliferation of deepfakes and other manipulated content. The realism achieved by these technologies raises urgent concerns about their potential misuse in sensitive areas like politics and economics. Moreover, if we simply use generated images as part of the training data, the trained model may largely degrade its quality (Shumailov et al., 2024), so it is essential to distinguish between natural images and generated ones. To deal with these potentially dire risks, various generated image detection methods have been developed. In this regard, a common approach is to consider generated image detection as a binary classification task. To train a binary classifier for detecting generated images, current methods typically require to collect numerous natural and generated images to construct a training dataset (Chai et al., 2020; Wang et al., 2020).

Although current methods have achieved exciting success, they often struggle to generalize well to images generated by unknown generative models. To promote the generalization ability on images generated by unknown generative models, one possible approach is to construct a more extensive training dataset by collecting more natural and generated images for training the binary classifier (Jeong et al., 2022; Tan et al., 2024). Besides collecting data, advanced methods propose to

[†]Correspondence to Bo Han (bhanml@comp.hkbu.edu.hk).

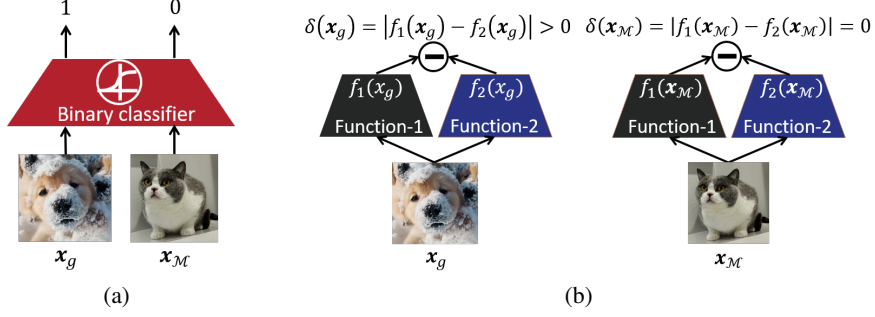


Figure 1: Comparison of (a): the existing framework, and (b): our proposed ConV. The binary classifier in (a) is trained using natural images x_M and generated images x_g , thereby, its efficacy relies on both the natural and generated data distributions. In contrast, the two functions in (b) are trained on natural data distribution, leading to the advantage of ConV: identifying generated images by fitting the distribution of natural images rather than that of generated images.

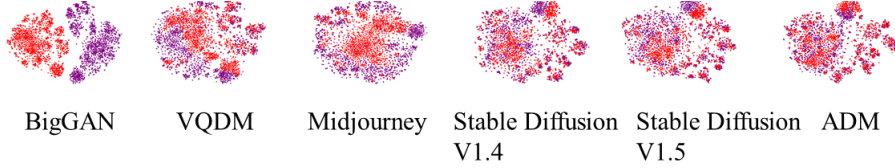


Figure 2: Generated images deviate from natural images' manifold, but the deviation decreases as generative model evolves. Red dots denote the feature representations of natural images, while purple dots represent those of generated images.

introduce pre-trained models as priors to promote the generalization ability. Some works, inspired by the recent success of large models, propose to detect generated images by leveraging features extracted by these large models (Ojha et al., 2023; Liu et al., 2024b), such as CLIP (Radford et al., 2021). Meanwhile, some works propose to leverage the reconstruction capabilities of pre-trained diffusion models (Wang et al., 2023; Ricker et al., 2024). Although these methods have achieved outstanding results, they require a lot of natural and generated images to train a binary classifier, making the current methods computationally intensive. Moreover, sustaining robust detection performance necessitates the continual collection of images generated by the latest generative models, which can be costly or even infeasible due to the inaccessibility of potential models, e.g., Sora OpenAI (2024).

Hence, the major challenge for the existing methods is ensuring that the binary classifier generalizes effectively across diverse unknown generative models. This stems from the fact that these binary classifiers are trained over natural and generated images to distinguish between these two types of images. Thus, the performance of these binary classifiers relies on the diversity of generated data. Unfortunately, it is challenging to determine whether a binary classifier trained over images generated by some diffusion models can generalize to those generated by other models. Their defects of heavy dependence on generated image distribution underscore the necessity of exploring a novel framework for generated image detection, where the detector's performance relies on the natural data distribution rather than the generated image distribution. However, this remains challenging, because the literature has yet to determine whether models training merely on natural images can be leveraged to distinguish between natural and generated images effectively, and if yes, how and why?

To address the challenge, we propose a novel framework for detecting generated images called **consistency verification (ConV)**. Using t-SNE, we visualize the low-dimensional manifold structure of feature representations extracted by DINOv2, which is trained solely on natural images. The embeddings of generated images exhibit distinct patterns compared to those of natural images, as illustrated in Figure 2, supporting the manifold disparities leveraged by our detection framework. To exploit this difference for detecting AI-generated images, as shown in Figure 1, we introduce two functions, aiming to detect generated images by ensuring that the outputs of these functions remain consistent for natural images but exhibit significant inconsistency for generated images. To this end, we establish a principle (see Eq. 6) to design these functions based on our theoretical analysis: outputs of these two functions are the same on the natural distribution while their gradients need to lie within two mutually orthogonal subspaces. This enables a training-free detection approach (see Eq. 12): if an image transformed along its data manifold induces a substantial change in the

loss value of a self-supervised model pre-trained over natural images, it is identified as generated. The advantage of ConV over existing methods is its reliance on fitting the natural data distribution rather than the distribution of generated images. However, as the generative model continues to develop, the deviation between the generated image and the natural image manifold will become smaller, as shown in Figure 2. To address this challenge, we propose actively projecting generated images onto the natural image manifold. The inherent diversity of natural images complicates explicit modeling of this manifold. To overcome this, we employ normalizing flow (Dinh et al., 2017; Kingma and Dhariwal, 2018) to transform the natural image manifold into a Gaussian distribution, enabling precise extrusion of generated images from the natural manifold. This approach significantly enhances detection performance. Comprehensive experiments across various benchmarks for generated image detection demonstrate the effectiveness of the proposed ConV (see Tables 1-7). To further verify the effectiveness of the proposed ConV, we collect images generated by Sora OpenAI (2024) and OpenSora Zheng et al. (2024) and compare ConV with baselines. The experiments demonstrate the efficacy and robustness of ConV against variations in generative models (see Table 2).

We summarize our main contributions as follows:

- We highlight the generalization issue of existing works: it is challenging to determine whether a detector trained over images generated by some diffusion models can generalize to those generated by other models. This motivates a promising direction to explore detectors whose detection ability relies solely on fitting the natural data distribution.
- We propose a novel framework for detecting generated images called **consistency verification** (ConV). This framework exploits the observed deviation of generated images from natural manifold and detect images by verifying consistency of two functions. The design of these functions is guided by our orthogonality principle. Namely, gradients of these functions need to lie within two mutually orthogonal subspaces (Eq 6). This enables a training-free approach to detecting generated images by leveraging the consistency of a pre-trained self-supervised model on images before and after perturbations along the data manifold.
- To further facilitate the deviation of the generated image, we explicitly extrude generated images out of natural manifold with the aid of normalized flow, enhancing the effectiveness of ConV. Extensive experiments conducted on various standard benchmarks and datasets collected from Sora demonstrate the effectiveness and robustness of the proposed method.

2 Consistency Verification

2.1 Motivation

Humans can distinguish generated images from natural images through some types of indescribable differences in patterns. Intuitively, humans know that if a natural image captures the same content as a given generated image, the natural image will be different. In contrast, if we degrade natural images along its data manifold, e.g., tiny affine transformation, the degraded natural images are still discriminated as natural images.

To formally characterize this discrepancy, we present the following notations. Let $\mathbf{x} \in \mathcal{X} \subset \mathbb{R}^d$ denote the image, where d denotes the dimension of images. To distinguish, we use \mathbf{x}_n and \mathbf{x}_g to denote the natural and generated image. In particular, for a given generated image \mathbf{x}_g , even if it captures similar content to a natural image \mathbf{x}_n , humans know they are distinguishable in certain ways. This can be formulated by projecting the generated image \mathbf{x}_g onto the point $\mathbf{x}_{\mathcal{M}(\mathbf{x}_g)}$ on the data manifold \mathcal{M} , i.e.,

$$\mathbf{x}_{\mathcal{M}(\mathbf{x}_g)} = \arg \min_{\mathbf{x}' \in \mathcal{M}} d(\mathbf{x}', \mathbf{x}_g), \mathbf{x}_{\mathcal{M}(\mathbf{x}_g)} \in \mathcal{M}, \mathbf{x}_g \notin \mathcal{M}, \quad (1)$$

where $\mathbf{x}_{\mathcal{M}(\mathbf{x}_g)}$ is the point closest to \mathbf{x}_g on the data manifold of natural images \mathcal{M} and d is a metric. Namely, images on the data manifold \mathcal{M} are considered natural, whereas those deviating from \mathcal{M} are regarded as generated.

In this context, the data manifold perspective provides an intuitive framework for understanding the difference. In particular, transforming natural image $\mathbf{x}_{\mathcal{M}}$ along the local tangent space $\mathcal{T}(\mathbf{x}_{\mathcal{M}})$,

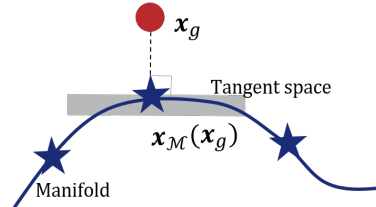


Figure 3: Illustration of projecting a generated image \mathbf{x}_g onto the data manifold \mathcal{M} .

leading to the fact that the degraded images are still on the data manifold. In contrast, even the discrepancy $d(\mathbf{x}_{\mathcal{M}}(\mathbf{x}_g), \mathbf{x}_g)$ is minimal, \mathbf{x}_g is considered as generated, because \mathbf{x}_g departs from the manifold. Intuitively, even a slight discrepancy between $\mathbf{x}_{\mathcal{M}}(\mathbf{x}_g)$ and \mathbf{x}_g allows us to identify the difference between a generated image and the corresponding natural image on the data manifold. Thus, we consider the discrepancy between a generated image and its closest natural image on the data manifold to represent the direction of the fastest departure from the manifold. This means that

$$\mathbf{v}^\top (\mathbf{x}_{\mathcal{M}}(\mathbf{x}_g) - \mathbf{x}_g) = 0, \quad \mathbf{v} \in \mathcal{T}(\mathbf{x}_{\mathcal{M}}(\mathbf{x}_g)). \quad (2)$$

This discrepancy inspires us to introduce two functions to detect generated images, where these two functions are related to the tangent space and the space orthogonal to the tangent space, respectively.

2.2 Objective

Aligning with the motivation, we introduce a two-function framework for generated image detection. In particular, we propose a consistency verification framework where the two introduced functions are devised to be consistent over natural images and inconsistent over generated images. Namely, this framework detects generated images by verifying the consistency of the two functions. Specifically, let $f_1(\cdot) : \mathbb{R}^d \rightarrow \mathbb{R}$ and $f_2(\cdot) : \mathbb{R}^d \rightarrow \mathbb{R}$ be the two functions. Then, the inconsistency $|f_1(\cdot) - f_2(\cdot)|$ between these two functions can be employed to detect generated images. Namely, generated images can be detected by $\mathbb{I}(|f_1(\cdot) - f_2(\cdot)| > \alpha)$ with the threshold α .

For images on the manifold, we make these two functions consistent by setting

$$\delta(\mathbf{x}_{\mathcal{M}}) = |f_1(\mathbf{x}_{\mathcal{M}}) - f_2(\mathbf{x}_{\mathcal{M}})| = 0, \quad (3)$$

where we denote $\mathbf{x}_{\mathcal{M}}(\mathbf{x}_g)$ as $\mathbf{x}_{\mathcal{M}}$ for simplicity. Then, the objective is to devise the two functions to ensure that the inconsistency over generated images is larger than that over the natural images, i.e., $\delta(\mathbf{x}_g) \geq \delta(\mathbf{x}_{\mathcal{M}})$. In this regard, we show that (with more details in the appendix)

$$\delta(\mathbf{x}_g) \geq ||\nabla f_1(\mathbf{x}_{\mathcal{M}})^\top (\mathbf{x}_g - \mathbf{x}_{\mathcal{M}})| - |\nabla f_2(\mathbf{x}_{\mathcal{M}})^\top (\mathbf{x}_g - \mathbf{x}_{\mathcal{M}})|| \geq 0 = \delta(\mathbf{x}_{\mathcal{M}}), \quad (4)$$

where equality holds if, and only if, the absolute values of the two quantities are identical. According to Eq. 4, enlarging the difference between these two terms, i.e., $|\nabla f_1(\mathbf{x}_{\mathcal{M}})^\top (\mathbf{x}_g - \mathbf{x}_{\mathcal{M}})|$ and $|\nabla f_2(\mathbf{x}_{\mathcal{M}})^\top (\mathbf{x}_g - \mathbf{x}_{\mathcal{M}})|$ will make the natural and generated images separable. Thus, the objective of consistency verification is to maximize one term and minimize the other term while keeping the output values of these two functions the same. This can be formalized by

$$\min_{f_1, f_2 \in \mathcal{F}} |\nabla f_1(\mathbf{x}_{\mathcal{M}})^\top (\mathbf{x}_g - \mathbf{x}_{\mathcal{M}})| - |\nabla f_2(\mathbf{x}_{\mathcal{M}})^\top (\mathbf{x}_g - \mathbf{x}_{\mathcal{M}})|, \text{ s.t. } f_1(\mathbf{x}_{\mathcal{M}}) = f_2(\mathbf{x}_{\mathcal{M}}), \quad (5)$$

where \mathcal{F} denotes a hypothesis space.

However, learning these two functions using Eq. 5 still relies on the generated data, i.e., \mathbf{x}_g . To decouple function optimization from the generated data distribution, we leverage orthogonality priors from the motivation 2.1 to provide design principles for these functions. According to the above discussion, one straightforward approach to realizing f_1 and f_2 is to devise these functions such that their gradients for the input lie in two orthogonal subspaces, i.e., the tangent space and the space orthogonal to the tangent space. This orthogonality principle can be formalized as,

$$\nabla f_1(\mathbf{x}_{\mathcal{M}}) \in \mathcal{O}(\mathbf{x}_{\mathcal{M}}), \quad \nabla f_2(\mathbf{x}_{\mathcal{M}}) \in \mathcal{T}(\mathbf{x}_{\mathcal{M}}), \quad f_1(\mathbf{x}_{\mathcal{M}}) = f_2(\mathbf{x}_{\mathcal{M}}) \quad (6)$$

where $\mathcal{O}(\mathbf{x}_{\mathcal{M}})$ denotes the subspace orthogonal to the tangent space $\mathcal{T}(\mathbf{x}_{\mathcal{M}})$. Then, we have

$$\delta(\mathbf{x}_g) \geq ||\nabla f_1(\mathbf{x}_{\mathcal{M}})^\top \mathbf{p}| - |\nabla f_2(\mathbf{x}_{\mathcal{M}})^\top \mathbf{p}|| = |\nabla f_1(\mathbf{x}_{\mathcal{M}})^\top \mathbf{p}| > 0 = \delta(\mathbf{x}_{\mathcal{M}}), \quad (7)$$

where $\mathbf{p} = \mathbf{x}_g - \mathbf{x}_{\mathcal{M}}$ denotes the difference between a generated image and its corresponding point on the data manifold, the equation holds due to the conclusion in Eq. 2, and the inequality holds because the probability that two vectors in the same space are orthogonal is zero. Consequently, the orthogonality principle ensures that these two functions are consistent on natural images, i.e., $f_1(\mathbf{x}_{\mathcal{M}}) = f_2(\mathbf{x}_{\mathcal{M}})$, while inconsistent on generated images, i.e., $|\delta(\mathbf{x}_g)| > |\delta(\mathbf{x}_{\mathcal{M}})| = 0$.

2.3 Realization

In this work, we propose a training-free approach to construct these two functions. The reason is twofold: i) our framework allows the training-free construction of these functions, and ii) we aim to

validate the effectiveness of the orthogonality principle without incurring significant energy costs, as fitting the distribution of natural data requires a lot of data and computing power for training.

Well-trained models are typically insensitive to the transformation along the data manifold [Simard et al. \(1991\)](#); [Bengio et al. \(2013\)](#); [Rifai et al. \(2011\)](#). This can be formalized as,

$$(\mathbf{v} - \mathbf{x}_{\mathcal{M}})^\top \frac{\partial \ell(\mathbf{x}_{\mathcal{M}})}{\partial \mathbf{x}_{\mathcal{M}}} \approx 0, \quad \mathbf{v} \in \mathcal{T}(\mathbf{x}_{\mathcal{M}}), \quad (8)$$

where \mathbf{v} stands for the point sampled from the tangent space $\mathcal{T}(\mathbf{x}_{\mathcal{M}})$ and $\ell(\cdot)$ is the loss function of a model. This implies that $\frac{\partial \ell(\mathbf{x}_{\mathcal{M}})}{\partial \mathbf{x}_{\mathcal{M}}}$ is orthogonal to the tangent space $\mathcal{T}(\mathbf{x}_{\mathcal{M}})$, which is consistent with the direction $\mathbf{p} = \mathbf{x}_g - \mathbf{x}_{\mathcal{M}}$, as shown in Eq 2. Hence, we propose to realize $f_1(\cdot)$ using a well-trained neural network. This means that both $\frac{\partial \ell(\mathbf{x}_{\mathcal{M}})}{\partial \mathbf{x}_{\mathcal{M}}}$ and \mathbf{p} lies in the subspace orthogonal to tangent space $\mathcal{T}(\mathbf{x}_{\mathcal{M}})$. This is consistent with the principle, i.e., $\nabla f_1(\mathbf{x}_{\mathcal{M}}) \in \mathcal{O}(\mathbf{x})$. We have

$$|\nabla f_1(\mathbf{x}_{\mathcal{M}})^\top \mathbf{p}| = \left| \frac{\partial \ell(\mathbf{x}_{\mathcal{M}})}{\partial \mathbf{x}_{\mathcal{M}}}^\top \mathbf{p} \right| = \left\| \frac{\partial \ell(\mathbf{x}_{\mathcal{M}})}{\partial \mathbf{x}_{\mathcal{M}}} \right\| \|\mathbf{p}\| |\cos(\frac{\partial \ell(\mathbf{x}_{\mathcal{M}})}{\partial \mathbf{x}_{\mathcal{M}}}, \mathbf{p})| > 0, \quad (9)$$

where $\mathbf{p} = \mathbf{x}_g - \mathbf{x}_{\mathcal{M}}$ is the difference between natural and generated images, and the last inequality holds because the probability that two vectors in the same space are orthogonal is zero. We propose to realize $f_1(\cdot)$ using models trained with self-supervised learning, which would avoid reliance on labels used in classification tasks. This is because obtaining the loss value of a classification model requires labels that could be hard to obtain in many practical scenarios.

For the second term, we will realize it using the orthogonality such that $\nabla f_2(\mathbf{x}_{\mathcal{M}}) \in \mathcal{T}(\mathbf{x}_{\mathcal{M}})$ or $|\nabla f_2(\mathbf{x}_{\mathcal{M}})^\top \mathbf{p}| = 0$. We achieve this by introducing the local tangent space into $\nabla f_2(\mathbf{x})$. To this end, we propose to realize f_2 using a composite function: $f_2 := f_1 \circ h$. This leads to the fact that

$$\nabla f_2(\mathbf{x}_{\mathcal{M}}) = \mathbf{J}_{h(\mathbf{x}_{\mathcal{M}})} \frac{\partial f_1(h(\mathbf{x}_{\mathcal{M}}))}{\partial h(\mathbf{x}_{\mathcal{M}})}, \quad (10)$$

where $\mathbf{J}_{h(\mathbf{x}_{\mathcal{M}})}$ is the Jacobian matrix of $h(\mathbf{x}_{\mathcal{M}})$. If $h(\cdot)$ models the transformation along local data manifold, $\mathbf{J}_{h(\mathbf{x}_{\mathcal{M}})}$ models the tangent space at point $\mathbf{x}_{\mathcal{M}}$. Then, we have

$$\nabla f_2(\mathbf{x}_{\mathcal{M}})^\top \mathbf{p} = \frac{\partial f_1(h(\mathbf{x}_{\mathcal{M}}))}{\partial h(\mathbf{x}_{\mathcal{M}})}^\top \mathbf{J}_{h(\mathbf{x}_{\mathcal{M}}}^\top \mathbf{p} = 0, \quad (11)$$

where $\mathbf{J}_{h(\mathbf{x})}^\top$ denotes the tangent space orthogonal to the vector $\mathbf{p} = \mathbf{x}_g - \mathbf{x}_{\mathcal{M}}$, see Eq. 2.

For the last term in the orthogonality principle, we should ensure that $f_1(\mathbf{x}_{\mathcal{M}}) = f_2(\mathbf{x}_{\mathcal{M}}) := f_1(h(\mathbf{x}_{\mathcal{M}}))$. There are numerous approaches to realize $h(\cdot)$. In this regard, we propose to leverage data transformation functions used in the training phase to realize $h(\cdot)$, because self-supervised models are trained to be insensitive to these transformations along local data manifold under various self-supervised learning scenarios ([Yu et al., 2023](#); [Jaderberg et al., 2015](#)). Thus, for a given input image \mathbf{x} , we can determine whether it is generated by calculating the consistency $\delta(\mathbf{x})$,

$$\delta(\mathbf{x}) = |f_1(\mathbf{x}) - f_1(h(\mathbf{x}))| \begin{cases} = 0, & \mathbf{x} \in \mathcal{M}, \\ > 0, & \mathbf{x} \notin \mathcal{M}. \end{cases} \quad (12)$$

Technically, our training-free realization is equal to verifying the robustness of a pre-trained self-supervised model $f_1(\cdot)$ against the data transformations $h(\cdot)$. Here, $f_1(\cdot)$ merely fits the natural data distribution, avoiding the reliance on the distribution of generated images.

2.4 Overview

An overview of the proposed consistency verification is presented in Figure 4. As shown in the figure, our method is training-free and seamlessly deployed in practical scenarios. Specifically, we merely download a neural network pre-trained with a self-supervised learning task over a large-scale dataset. Subsequently, we obtain the loss values of both the original and transformed images. Ultimately, images are identified as generated if the difference between loss values exceeds a predetermined threshold. We can apply multiple random transformations and compute corresponding loss function values if computational resources allow. Intuitively, this would result in more accurate detection performance, which is fortunately consistent with our experiments, see Figure 5.

Negative samples are widely used in self-supervised learning, which could increase the computational cost of generated image detection. Inspired by a recent work [Oquab et al. \(2024\)](#), we calculate the similarity of representation $\mathbf{r} = \phi(\mathbf{x})$, where $\phi(\cdot)$ is the feature extractor of a self-supervised model. The feasibility results from the objective function used in self-supervised learning,

$$\log P(\mathbf{x}) = \log \frac{e^{(\mathbf{r}^\top \mathbf{r}_h / \tau)}}{\sum_{\mathbf{z}_-} e^{(\mathbf{r}^\top \mathbf{r}_- / \tau)} + e^{(\mathbf{r}^\top \mathbf{r}_h / \tau)}} = \log \frac{1}{\sum_{\mathbf{z}_-} e^{(\mathbf{r}^\top \mathbf{r}_- / \tau) - (\mathbf{r}^\top \mathbf{r}_h / \tau)} + 1}, \quad (13)$$

where \mathbf{r}_h is the representation of $h(\mathbf{x})$ and \mathbf{r}_- denotes the representation of negative samples. Thus, we can employ the similarity between representations, i.e., $\mathbf{r}^\top \mathbf{r}_h$, as a surrogate of loss value. This avoids the use of negative samples. Note that applying a softmax function to the representation \mathbf{r} leads to the objective function used in previous works [Caron et al. \(2021\)](#); [Oquab et al. \(2024\)](#). In this context, the high similarity between the representation of images and transformed images means the consistency between functions, i.e., detected as natural images.

2.5 Flow-Based Manifold Extrusion

Although generated images, such as those generated by GANs or diffusion models, deviate from the manifold of natural images, this deviation is often subtle, making differentiation challenging. To address this, we aim to actively extrude generated images from the natural image manifold through targeted training, thereby amplifying their separation. However, the challenge comes from the diversity of natural images, which leads to their extremely complex manifolds. This complexity prevents direct modeling of natural manifold. To address this challenge, we propose **F-ConV** to leverage normalizing flows ([Dinh et al., 2017](#)) to reshape the natural manifold into a Gaussian distribution, facilitating robust differentiation.

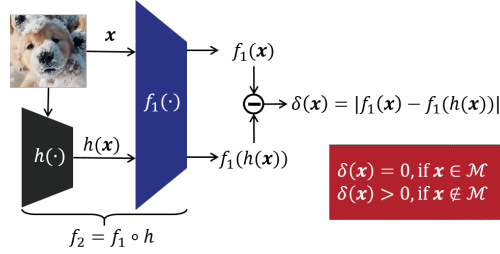


Figure 4: Framework of consistency verification.

The goal of the normalizing flows is to learn an invertible mapping f , which transforms a complex distribution $P_X(v)$ into a simple one $P_Z(z)$: $z = f(v)$ and v is the image feature extracted by the fundamental model: $v = f(x)$. The distribution $P_Z(z)$ is commonly chosen to be a standard Gaussian. Therefore, the objective function for normalizing flow is: Formally, let $f : \mathbb{R}^d \rightarrow \mathbb{R}^d$ be the invertible transformation, mapping an input feature v to a latent variable $z = f(v)$, where $z \sim \mathcal{N}(0, I)$. According to the change of variable formula, the log-likelihood of v is:

$$\log p(v) = \log p_z(f(v)) + \log \left| \det \left(\frac{\partial f(v)}{\partial v} \right) \right|, \quad (14)$$

where $\left| \det \left(\frac{\partial f(v)}{\partial v} \right) \right|$ is the determinant of the Jacobian matrix of f at v . In order to enforce the deviation of the generated image, we introduce the following loss function:

$$\mathcal{L} = \underbrace{-\mathbb{E}_{v \sim \mathcal{D}_n} \log p(v) + \mathbb{E}_{v \sim \mathcal{D}_g} \log p(v)}_{\text{Shaping Loss}} - \underbrace{\mathbb{E}_{v \sim \mathcal{D}_n} \cos(f(v); f(T(v))) + \mathbb{E}_{v \sim \mathcal{D}_g} \cos(f(v); f(T(v)))}_{\text{Consistency Loss}}, \quad (15)$$

where \mathcal{D}_n and \mathcal{D}_g denote the distributions of natural and generated images, respectively. $T(v)$ is the feature of transformed image: $T(v) = f(h(x))$. Intuitively, shaping loss pushes the generated images away from natural images' manifold, while the consistency loss amplifies consistency disparity between natural images and generated images. Upon completion of training, we make a judgment of an image by assessing the feature consistency between the original image and its transformed image, as well as its likelihood under the normalizing flow model.

Table 1: Detection performance (%) on ImageNet. Bold numbers are superior results. We compare training methods and training-free methods separately.

Methods	ADM		ADMG		LDM		DiT		BigGAN		GigaGAN		StyleGAN XL		RQ-Transformer		Mask GIT		Average	
	AUROC	AP	AUROC	AP	AUROC	AP	AUROC	AP	AUROC	AP	AUROC	AP	AUROC	AP	AUROC	AP	AUROC	AP	AUROC (†)	AP (†)
Training-based Methods																				
CNNspot	62.25	63.13	63.28	62.27	63.16	64.81	62.85	61.16	85.71	84.93	74.85	71.45	68.41	68.67	61.83	62.91	60.98	61.69	67.04	66.78
Ojha	83.37	82.95	79.60	78.15	80.35	79.71	82.93	81.72	93.07	92.77	87.45	84.88	85.36	83.15	85.19	84.22	90.82	90.71	85.35	84.25
DIRE	51.82	50.29	53.14	52.96	52.83	51.84	54.67	55.10	51.62	50.83	50.70	50.27	50.95	51.36	55.95	54.83	52.58	52.10	52.70	52.18
NPR	85.68	80.86	84.34	79.79	91.98	86.96	86.15	81.26	89.73	84.46	82.21	78.20	84.13	78.73	80.21	73.21	89.61	84.15	86.00	80.84
DRCT	90.26	90.07	85.74	83.85	90.24	89.88	88.27	89.06	95.87	94.99	86.89	86.12	89.11	88.39	92.38	92.41	94.44	94.47	90.36	89.92
FatFormer	91.77	90.36	83.58	83.17	92.58	92.06	86.93	85.14	98.76	98.47	97.65	98.02	97.64	97.57	96.55	95.96	97.65	97.27	93.68	93.11
F-ConV	92.74	91.65	88.51	87.67	88.87	88.47	85.94	84.88	98.94	98.98	98.14	98.72	98.52	98.38	96.79	96.33	95.52	95.38	93.77	93.38
Training-free Methods																				
AEROBLADA	55.61	54.26	61.57	56.58	62.67	60.93	85.88	87.71	44.36	45.66	47.39	48.14	47.28	48.54	67.05	67.69	48.05	48.75	57.87	57.85
ConV	88.89	86.60	82.46	79.83	78.94	75.88	75.25	70.11	92.83	92.05	91.89	90.93	92.15	91.82	93.02	91.26	88.79	87.88	87.13	85.15

Table 2: Detection performance (%) on Sora.

Models	CNNspot		Ojha		NPR		DRCT		DIRE		FatFormer		F-ConV		AEROBLADA		ConV	
	AUROC	AP	AUROC	AP	AUROC	AP	AUROC	AP	AUROC	AP	AUROC	AP	AUROC	AP	AUROC	AP	AUROC	AP
Sora	52.85	53.29	77.06	80.69	51.92	50.25	82.53	82.28	52.83	52.16	89.95	87.64	91.74	89.95	57.13	58.00	87.74	88.85
Open Sora	50.14	51.38	67.05	68.67	50.25	51.84	81.79	80.11	53.66	52.98	88.76	87.99	90.16	87.38	55.79	62.37	82.84	85.24
Average	51.50	52.84	72.06	74.68	51.09	51.05	82.16	81.20	53.25	52.57	89.36	87.82	90.95	88.67	56.46	60.19	85.29	87.05

3 Experiments

3.1 Experiment setup

Datasets. Following previous work (Chen et al., 2024), we evaluate ConV on several benchmarks: **ImageNet** (Deng et al., 2009), **LSUN-BEDROOM** (Yu et al., 2015), **GenImage** (Zhu et al., 2023b) and **DRCT2M** (Chen et al., 2024). Detailed dataset description can be found in the Appendix G.

Besides these image dataset, current advancements in generative technology have significantly enhanced the realism of synthetic videos (Khachatrian et al., 2023; Blattmann et al., 2023), thereby raising substantial concerns regarding trust in digital media. Moreover, the inaccessibility of their parameters and even their architectures underscores the necessity of verifying the generalization capability of newly proposed detection methods over these generative models. To verify whether the proposed ConV generalizes to these challenging scenarios, we download videos generated by these models and detect images sampled from these videos. Since we currently cannot access the generative model used in Sora (OpenAI, 2024), we gathered several videos and extracted 1,000 frames. Additionally, we generate 100 videos through the open-source OpenSora project (Zheng et al., 2024), extracting 5,000 frames. With these images used as generated images and Laion serving as natural images, we further evaluate ConV’s performance and compare it with baselines.

Baselines and evaluation metrics. We use training-free and training-based methods as baselines. For training-free methods, we take AEROBLADE (Ricker et al., 2024) as our baseline. For training-based methods, we take DIRE (Wang et al., 2023), CNNspot (Wang et al., 2020), Ojha (Ojha et al., 2023), DRCT (Chen et al., 2024), FatFormer (Liu et al., 2024a) and NPR (Tan et al., 2024) as baselines. For some baselines, we get the results reported in their papers, including Frank (Frank et al., 2020), Durall et al. (Durall et al., 2020), Patchfor (Chai et al., 2020), F3Net (Qian et al., 2020), SelfBland (Shiohara and Yamasaki, 2022), GANDetection (Mandelli et al., 2022), LGrad (Tan et al., 2023), DeiT-S (Touvron et al., 2021), Swin-T (Liu et al., 2021), Spec (Zhang et al., 2019), GenDet (Zhu et al., 2023a) and GramNet (Liu et al., 2020). And following previous works (Ojha et al., 2023; Tan et al., 2024), we mainly use the following metrics: (1) the average precision (AP); (2) the area under the receiver operating characteristic curve (AUROC) and (3) the classification accuracy (ACC).

Implementation details. In our experiments, we use the DINOv2 to instantiate $f_1(\cdot)$ and common transformation (details are in Appendix E) to realize $h(\cdot)$. There are four pre-trained DINOv2 models, i.e., ViT-S/14, ViT-B/14, ViT-L/14, and ViT-g/14, achieving exciting AUROC performance on ImageNet benchmark: 62.84, 78.58, 87.13, and 85.97, respectively.

To balance detection performance and efficiency, we use DINOv2 ViT-L/14 in the following experiments. Meanwhile, We leverage data augmentations used in the training phase to realize the

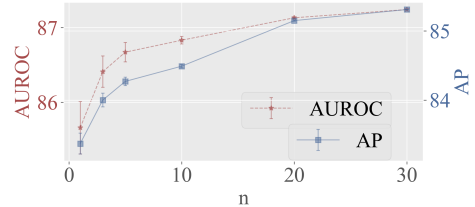


Figure 5: ConV with multiple forward passes.

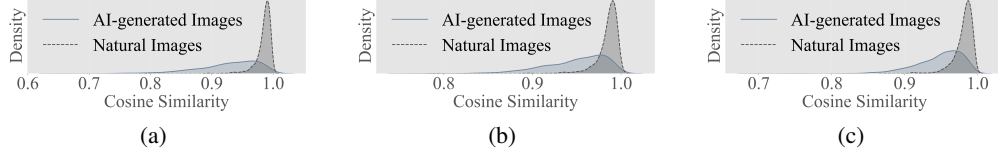


Figure 7: Cosine similarity between features of \mathbf{x} and $h(\mathbf{x})$, where generated images are generated by a) BigGAN, b) ADM, and c) DDPM.

function $h(\cdot)$ in $f_2 = f_1 \circ h$, including geometric augmentation, color jitter, and Gaussian blur. Since data augmentation is randomized, to enhance performance, we apply the function n times to a single test image. As illustrated in Figure 5, increasing n correlates with improved detection performance. However, to maintain detection efficiency, we set $n = 20$ in our experiments. In practical applications, if multiple machines are available, we can leverage parallel processing to implement multiple transformations in a single forward pass to achieve better detection performance. In our experiments, we report the average results under five different random seeds. For F-ConV, we train a RealNVP (Dinh et al., 2017) on the top of DINOv2 ViT-L/14, which consists of 2 coupling blocks with fully connected networks as internal functions. The model is trained using AdamW with a learning rate of $1e-5$. More detailed implementation information is provided in Appendix F.

3.2 Main Result

Comparison on public benchmarks. We conduct comparative experiments across a comprehensive suite of standard benchmarks. As shown in Tables 1, 7, 9 and 8, without training, ConV achieves comparable performance to training methods. And ConV performs better than some of advanced training methods in out-of-distribution generative models. When further extruding the generated image out of natural images’ manifold through training, F-ConV achieves the best performance, illustrating the effectiveness of the generalization ability of the proposed method.

Comparison on Sora. We further evaluate ConV’s performance on videos generated by unknown models. As shown in Table 2, ConV demonstrates the best performance on images generated by these unknown generative models, previous methods. These results highlight the effectiveness and robustness of the proposed ConV.

Illustration of the effectiveness. We visualize the features of natural image \mathbf{x}_n and generated image \mathbf{x}_g as well as the features of their augmented versions, i.e., $h(\mathbf{x}_n)$ and $h(\mathbf{x}_g)$. We extract features of \mathbf{x}_n , \mathbf{x}_g , $h(\mathbf{x}_n)$ and $h(\mathbf{x}_g)$ using DINOv2 and use t-SNE to visualize these features. To avoid the effect of class, all images are sampled from the same class for visualization. As shown in Figure 6, the conclusions are mainly twofold. First, the features of natural (\mathbf{x}_n) and augmented ($h(\mathbf{x}_n)$) images can be distinguished from those of generated images and their augmented versions, showing DINOv2’s ability to differentiate between natural and generated images. This provides a promising direction to leverage DINOv2 for generated image detection. Second, the separation between a generated image and its augmented version in the representation space is more pronounced than that of natural images. The feature of $h(\mathbf{x}_n)$ is similar to that of \mathbf{x}_n , i.e., features of $h(\mathbf{x}_n)$ substantially overlap with those of the natural image \mathbf{x}_n . In contrast, the features of $h(\mathbf{x}_g)$ generally fail to fully encompass those of the generated images \mathbf{x}_g . Aligning with this, ConV effectively distinguishes natural and generated images by calculating feature similarity between the original and augmented images. This is consistent with the conclusion from Figure 7 showing the similarity between features of \mathbf{x} and $h(\mathbf{x})$.

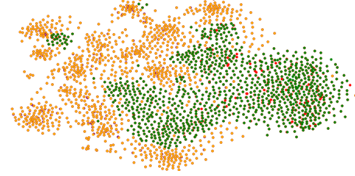


Figure 6: t-SNE visualization of features extracted by DINOv2. Natural image features (\cdot and \cdot) remain nearly unchanged after transformations, causing overlap, while generated image features (\cdot and \cdot) show notable shifts.

3.3 Discussion

When deploying a detector to identify generated images, it is crucial to consider practical environments or even a threat model. Specifically, images are often perturbed in practical scenarios, affecting detection performance. For instance, JPEG compression is a common mechanism due to the spread of images on the Internet. Moreover, AI-generated images may undergo post-processing to evade detection mechanisms. If a detection method is sensitive to some perturbations, the vulnerability

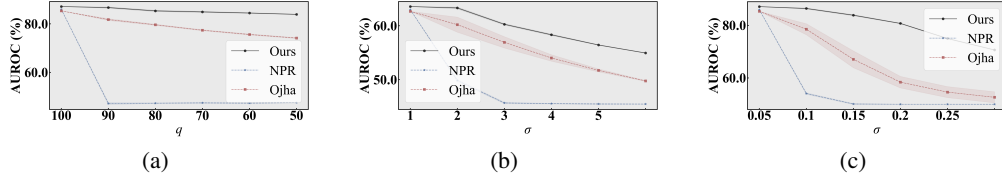


Figure 8: Detection performance under various perturbations: a) JPEG compression, b) Gaussian blur, and c) Gaussian noise.

would limit the applications in many practical scenarios. Thus, robustness to various perturbations is an essential metric in generated image detection. To verify the robustness of the proposed ConV, we process both natural and generated images by introducing some degradation mechanisms. Unless otherwise stated, experiments are conducted on the ImageNet dataset.

Following previous works (Ricker et al., 2024), we evaluate the robustness of ConV in three perturbations, including JPEG compression (with quality q), Gaussian blur, and Gaussian noise (both with standard deviation σ). As shown in Figure 8, ConV achieves the best performance. We find that training-free methods usually show better robustness than training-based methods. Specifically, although NPR achieves promising results on clean images, its performance degrades drastically under perturbations. This may stem from its reliance on the relationship between pixels. Namely, various small perturbations can change its features, causing its performance to degrade drastically. In contrast, ConV leverages the generalization ability of the pre-trained self-supervised model and is robust under various perturbations, making it suitable for a wider range of applications. Besides, we verify the efficacy of the proposed method using more pre-trained models with results in Appendix N. The results demonstrate that our method can be applied for various pre-trained models.

4 Related Works

Generated images detection. With the rapid advancements in generative models (Brock et al., 2019), the generation of highly realistic images has become increasingly feasible, thereby creating an urgent demand for effective algorithms to detect such generated images. Previous work (Frank et al., 2020) has usually focused on training a specialized binary classification neural network to distinguish between natural and generated images. CNNspot (Wang et al., 2020) finds that with specific data augmentation, a standard image classifier trained on ProGAN is able to generalize to other architectures. However, Ojha (Ojha et al., 2023) shows that the generalizability does not extend to unseen families of generative models. To this end, they propose to train classifiers in CLIP’s representation space to obtain stronger generalisability. DIRE (Wang et al., 2023) uses the reconstruction error of an image on a diffusion model to train the classifier. However, training-based approaches often suffer from generalizability issues and high computational costs. To address these limitations, several training-free methods have recently been proposed. AEROBLADE (Tan et al., 2024) performs the detection by calculating the reconstruction error with the autoencoder used in latent diffusion models (Rombach et al., 2022). However, understanding the underlying mechanisms that enable these approaches to perform well on images generated by unknown generative models remains challenging. On the contrary, our method explicitly maps how the generated images are detected. Thus, exhibiting good generalization performance on images generated by unknown models is in line with expectations. Fortunately, our experiments on images generated by Sora and OpenSora provide effective support, see Table 2.

Manifold learning. Manifold learning Cayton et al. (2008) assumes that real-world data presented in high dimensional spaces are expected to concentrate in the vicinity of a manifold \mathcal{M} of much lower dimensionality, embedded in high dimensional space. Namely, the probability mass tends to concentrate in regions with significantly lower dimensionality than the original space in which the data resides Bengio et al. (2013). In this context, tangent directions/spaces of the manifold. The tangent space of the manifold changes as the point-of-interest moves on the manifold, as shown in Figure 3. The local tangent space at a point on the manifold can be considered as capturing locally valid transformations, i.e., transformed points are still on the data manifold. Intuitively, a well-trained model is invariant to transformations along the tangent space Simard et al. (1991), which is mathematically equal to the orthogonality between vectors from the tangent space and the gradient of the model’s loss with respect to the input, i.e., Eq. 8.

5 Conclusion

In this work, we propose ConV, a novel framework for detecting generated images. Unlike existing methods that rely heavily on substantial datasets of natural and generated images, ConV relies solely on the natural image distribution. This is achieved by designing two functions whose outputs exhibit consistency for natural images but significant inconsistency for generated images. Extensive experiments on diverse benchmarks and images generated by a currently inaccessible model, i.e., Sora, have demonstrated ConV’s superior performance.

Acknowledgments

JN and BH were supported by NSFC General Program No. 62376235, RGC Young Collaborative Research Grant No. C2005-24Y, RGC General Research Fund No. 12200725, Guangdong Basic and Applied Basic Research Foundation Nos. 2022A1515011652 and 2024A151501239, and HKBU CSD Departmental Incentive Scheme. XMT was supported by NSFC No. 62222117. MMG was supported by ARC DP240102088 and WIS-MBZUAI 142571. KZ acknowledges the support from NSF Award No. 2229881, AI Institute for Societal Decision Making (AI-SDM), the National Institutes of Health (NIH) under Contract R01HL159805, and grants from Qures AI, Florin Court Capital, and MBZUAI-WIS Joint Program. YGZ was funded by Inno HK Generative AI R&D Center.

References

- Batifol, S., Blattmann, A., Boesel, F., Consul, S., Diagne, C., Dockhorn, T., English, J., English, Z., Esser, P., Kulal, S., et al. (2025). Flux. 1 kontext: Flow matching for in-context image generation and editing in latent space. *arXiv e-prints*, pages arXiv–2506.
- Bengio, Y., Courville, A., and Vincent, P. (2013). Representation learning: A review and new perspectives. *IEEE transactions on pattern analysis and machine intelligence*, 35(8):1798–1828.
- Blattmann, A., Rombach, R., Ling, H., Dockhorn, T., Kim, S. W., Fidler, S., and Kreis, K. (2023). Align your latents: High-resolution video synthesis with latent diffusion models. In *The IEEE / CVF Computer Vision and Pattern Recognition Conference, CVPR*.
- Brock, A., Donahue, J., and Simonyan, K. (2019). Large scale GAN training for high fidelity natural image synthesis. In *International Conference on Learning Representations, ICLR*.
- Caron, M., Misra, I., Mairal, J., Goyal, P., Bojanowski, P., and Joulin, A. (2020). Unsupervised learning of visual features by contrasting cluster assignments. In *Advances in Neural Information Processing Systems, NeurIPS*.
- Caron, M., Touvron, H., Misra, I., Jégou, H., Mairal, J., Bojanowski, P., and Joulin, A. (2021). Emerging properties in self-supervised vision transformers. In *IEEE/CVF International Conference on Computer Vision, ICCV*.
- Cayton, L. et al. (2008). *Algorithms for manifold learning*. eScholarship, University of California.
- Chai, L., Bau, D., Lim, S., and Isola, P. (2020). What makes fake images detectable? understanding properties that generalize. In *Proceedings of the European Conference on Computer Vision, ECCV*.
- Chen, B., Zeng, J., Yang, J., and Yang, R. (2024). DRCT: diffusion reconstruction contrastive training towards universal detection of diffusion generated images. In *International Conference on Machine Learning, ICML*.
- Deng, J., Dong, W., Socher, R., Li, L., Li, K., and Fei-Fei, L. (2009). Imagenet: A large-scale hierarchical image database. In *The IEEE / CVF Computer Vision and Pattern Recognition Conference, CVPR*.
- Dhariwal, P. and Nichol, A. Q. (2021). Diffusion models beat gans on image synthesis. In *Advances in Neural Information Processing Systems, NeurIPS*.
- Dinh, L., Sohl-Dickstein, J., and Bengio, S. (2017). Density estimation using real NVP. In *International Conference on Learning Representations, ICLR*.

- Durall, R., Keuper, M., and Keuper, J. (2020). Watch your up-convolution: CNN based generative deep neural networks are failing to reproduce spectral distributions. In *The IEEE / CVF Computer Vision and Pattern Recognition Conference, CVPR*.
- Frank, J., Eisenhofer, T., Schönherr, L., Fischer, A., Kolossa, D., and Holz, T. (2020). Leveraging frequency analysis for deep fake image recognition. In *International Conference on Machine Learning, ICML*.
- He, K., Fan, H., Wu, Y., Xie, S., and Girshick, R. B. (2020). Momentum contrast for unsupervised visual representation learning. In *The IEEE / CVF Computer Vision and Pattern Recognition Conference, CVPR*.
- Jaderberg, M., Simonyan, K., Zisserman, A., and Kavukcuoglu, K. (2015). Spatial transformer networks. In *Advances in Neural Information Processing Systems, NeurIPS*, pages 2017–2025.
- Jeong, Y., Kim, D., Ro, Y., Kim, P., and Choi, J. (2022). Fingerprintnet: Synthesized fingerprints for generated image detection. In *Proceedings of the European Conference on Computer Vision, ECCV*.
- Karras, T., Laine, S., and Aila, T. (2019). A style-based generator architecture for generative adversarial networks. In *The IEEE / CVF Computer Vision and Pattern Recognition Conference, CVPR*.
- Khachatryan, L., Movsisyan, A., Tadevosyan, V., Henschel, R., Wang, Z., Navasardyan, S., and Shi, H. (2023). Text2video-zero: Text-to-image diffusion models are zero-shot video generators. In *IEEE/CVF International Conference on Computer Vision, ICCV*.
- Kingma, D. P. and Dhariwal, P. (2018). Glow: Generative flow with invertible 1x1 convolutions. In *Advances in Neural Information Processing Systems, NeurIPS*.
- Liu, H., Tan, Z., Tan, C., Wei, Y., Wang, J., and Zhao, Y. (2024a). Forgery-aware adaptive transformer for generalizable synthetic image detection. In *IEEE/CVF Conference on Computer Vision and Pattern Recognition, CVPR*.
- Liu, H., Tan, Z., Tan, C., Wei, Y., Zhao, Y., and Wang, J. (2024b). Forgery-aware adaptive transformer for generalizable synthetic image detection. In *The IEEE / CVF Computer Vision and Pattern Recognition Conference, CVPR*.
- Liu, Z., Lin, Y., Cao, Y., Hu, H., Wei, Y., Zhang, Z., Lin, S., and Guo, B. (2021). Swin transformer: Hierarchical vision transformer using shifted windows. In *IEEE/CVF International Conference on Computer Vision, ICCV*.
- Liu, Z., Qi, X., and Torr, P. H. S. (2020). Global texture enhancement for fake face detection in the wild. In *The IEEE / CVF Computer Vision and Pattern Recognition Conference, CVPR*.
- Mandelli, S., Bonettini, N., Bestagini, P., and Tubaro, S. (2022). Detecting gan-generated images by orthogonal training of multiple cnns. In *International Conference on Image Processing, ICIP*.
- Ojha, U., Li, Y., and Lee, Y. J. (2023). Towards universal fake image detectors that generalize across generative models. In *The IEEE / CVF Computer Vision and Pattern Recognition Conference, CVPR*.
- OpenAI (2024). Sora: Creating video from text.
- Oquab, M., Darcet, T., Moutakanni, T., Vo, H. V., Szafraniec, M., Khalidov, V., Fernandez, P., Haziza, D., Massa, F., El-Nouby, A., Assran, M., Ballas, N., Galuba, W., Howes, R., Huang, P., Li, S., Misra, I., Rabbat, M., Sharma, V., Synnaeve, G., Xu, H., Jégou, H., Mairal, J., Labatut, P., Joulin, A., and Bojanowski, P. (2024). Dinov2: Learning robust visual features without supervision. *Trans. Mach. Learn. Res.*
- Qian, Y., Yin, G., Sheng, L., Chen, Z., and Shao, J. (2020). Thinking in frequency: Face forgery detection by mining frequency-aware clues. In *Proceedings of the European Conference on Computer Vision, ECCV*.

- Radford, A., Kim, J. W., Hallacy, C., Ramesh, A., Goh, G., Agarwal, S., Sastry, G., Askell, A., Mishkin, P., Clark, J., Krueger, G., and Sutskever, I. (2021). Learning transferable visual models from natural language supervision. In *International Conference on Machine Learning, ICML*.
- Ricker, J., Lukovnikov, D., and Fischer, A. (2024). AEROBLADE: training-free detection of latent diffusion images using autoencoder reconstruction error. In *The IEEE / CVF Computer Vision and Pattern Recognition Conference, CVPR*.
- Rifai, S., Dauphin, Y. N., Vincent, P., Bengio, Y., and Muller, X. (2011). The manifold tangent classifier. *Advances in neural information processing systems*, 24.
- Rombach, R., Blattmann, A., Lorenz, D., Esser, P., and Ommer, B. (2022). High-resolution image synthesis with latent diffusion models. In *The IEEE / CVF Computer Vision and Pattern Recognition Conference, CVPR*.
- Shiohara, K. and Yamasaki, T. (2022). Detecting deepfakes with self-blended images. In *The IEEE / CVF Computer Vision and Pattern Recognition Conference, CVPR*.
- Shumailov, I., Shumaylov, Z., Zhao, Y., Papernot, N., Anderson, R. J., and Gal, Y. (2024). AI models collapse when trained on recursively generated data. *Nature*.
- Simard, P., Victorri, B., LeCun, Y., and Denker, J. (1991). Tangent prop-a formalism for specifying selected invariances in an adaptive network. *Advances in neural information processing systems*, 4.
- Stein, G., Cresswell, J. C., Hosseinzadeh, R., Sui, Y., Ross, B. L., Villecroze, V., Liu, Z., Caterini, A. L., Taylor, J. E. T., and Loaiza-Ganem, G. (2023). Exposing flaws of generative model evaluation metrics and their unfair treatment of diffusion models. In *Advances in Neural Information Processing Systems, NeurIPS*.
- Tan, C., Liu, H., Zhao, Y., Wei, S., Gu, G., Liu, P., and Wei, Y. (2024). Rethinking the up-sampling operations in cnn-based generative network for generalizable deepfake detection. In *The IEEE / CVF Computer Vision and Pattern Recognition Conference, CVPR*.
- Tan, C., Zhao, Y., Wei, S., Gu, G., and Wei, Y. (2023). Learning on gradients: Generalized artifacts representation for gan-generated images detection. In *The IEEE / CVF Computer Vision and Pattern Recognition Conference, CVPR*.
- Touvron, H., Cord, M., Douze, M., Massa, F., Sablayrolles, A., and Jégou, H. (2021). Training data-efficient image transformers & distillation through attention. In *International Conference on Machine Learning, ICML*.
- Wang, S., Wang, O., Zhang, R., Owens, A., and Efros, A. A. (2020). Cnn-generated images are surprisingly easy to spot... for now. In *The IEEE / CVF Computer Vision and Pattern Recognition Conference, CVPR*.
- Wang, Z., Bao, J., Zhou, W., Wang, W., Hu, H., Chen, H., and Li, H. (2023). DIRE for diffusion-generated image detection. In *IEEE/CVF International Conference on Computer Vision, ICCV*.
- Yang, Z., Xu, Q., Bao, S., Wen, P., He, Y., Cao, X., and Huang, Q. (2023). Auc-oriented domain adaptation: From theory to algorithm. *IEEE Transactions on Pattern Analysis and Machine Intelligence*.
- Yu, F., Zhang, Y., Song, S., Seff, A., and Xiao, J. (2015). LSUN: construction of a large-scale image dataset using deep learning with humans in the loop. *CoRR*.
- Yu, H., Qin, Z., Hou, J., Saleh, M., Li, D., Busam, B., and Ilic, S. (2023). Rotation-invariant transformer for point cloud matching. In *The IEEE / CVF Computer Vision and Pattern Recognition Conference, CVPR*.
- Zhang, X., Karaman, S., and Chang, S. (2019). Detecting and simulating artifacts in GAN fake images. In *International Workshop on Information Forensics and Security, WIFS*.
- Zheng, Z., Peng, X., Yang, T., Shen, C., Li, S., Liu, H., Zhou, Y., Li, T., and You, Y. (2024). Open-sora: Democratizing efficient video production for all.

- Zhu, M., Chen, H., Huang, M., Li, W., Hu, H., Hu, J., and Wang, Y. (2023a). Gendet: Towards good generalizations for ai-generated image detection. *arXiv preprint arXiv:2312.08880*.
- Zhu, M., Chen, H., Yan, Q., Huang, X., Lin, G., Li, W., Tu, Z., Hu, H., Hu, J., and Wang, Y. (2023b). Genimage: A million-scale benchmark for detecting ai-generated image. In *Advances in Neural Information Processing Systems, NeurIPS*.

NeurIPS Paper Checklist

1. Claims

Question: Do the main claims made in the abstract and introduction accurately reflect the paper's contributions and scope?

Answer: [\[Yes\]](#) ,

Justification: The main claims made in the abstract and introduction accurately reflects the paper's contributions and scope.

Guidelines:

- The answer NA means that the abstract and introduction do not include the claims made in the paper.
- The abstract and/or introduction should clearly state the claims made, including the contributions made in the paper and important assumptions and limitations. A No or NA answer to this question will not be perceived well by the reviewers.
- The claims made should match theoretical and experimental results, and reflect how much the results can be expected to generalize to other settings.
- It is fine to include aspirational goals as motivation as long as it is clear that these goals are not attained by the paper.

2. Limitations

Question: Does the paper discuss the limitations of the work performed by the authors?

Answer: [\[Yes\]](#) ,

Justification: Limitations are discussed in Appendix [B](#).

Guidelines:

- The answer NA means that the paper has no limitation while the answer No means that the paper has limitations, but those are not discussed in the paper.
- The authors are encouraged to create a separate "Limitations" section in their paper.
- The paper should point out any strong assumptions and how robust the results are to violations of these assumptions (e.g., independence assumptions, noiseless settings, model well-specification, asymptotic approximations only holding locally). The authors should reflect on how these assumptions might be violated in practice and what the implications would be.
- The authors should reflect on the scope of the claims made, e.g., if the approach was only tested on a few datasets or with a few runs. In general, empirical results often depend on implicit assumptions, which should be articulated.
- The authors should reflect on the factors that influence the performance of the approach. For example, a facial recognition algorithm may perform poorly when image resolution is low or images are taken in low lighting. Or a speech-to-text system might not be used reliably to provide closed captions for online lectures because it fails to handle technical jargon.
- The authors should discuss the computational efficiency of the proposed algorithms and how they scale with dataset size.
- If applicable, the authors should discuss possible limitations of their approach to address problems of privacy and fairness.
- While the authors might fear that complete honesty about limitations might be used by reviewers as grounds for rejection, a worse outcome might be that reviewers discover limitations that aren't acknowledged in the paper. The authors should use their best judgment and recognize that individual actions in favor of transparency play an important role in developing norms that preserve the integrity of the community. Reviewers will be specifically instructed to not penalize honesty concerning limitations.

3. Theory assumptions and proofs

Question: For each theoretical result, does the paper provide the full set of assumptions and a complete (and correct) proof?

Answer: [\[Yes\]](#)

Justification: The paper provides a full set of assumptions and a complete proof.

Guidelines:

- The answer NA means that the paper does not include theoretical results.
- All the theorems, formulas, and proofs in the paper should be numbered and cross-referenced.
- All assumptions should be clearly stated or referenced in the statement of any theorems.
- The proofs can either appear in the main paper or the supplemental material, but if they appear in the supplemental material, the authors are encouraged to provide a short proof sketch to provide intuition.
- Inversely, any informal proof provided in the core of the paper should be complemented by formal proofs provided in appendix or supplemental material.
- Theorems and Lemmas that the proof relies upon should be properly referenced.

4. Experimental result reproducibility

Question: Does the paper fully disclose all the information needed to reproduce the main experimental results of the paper to the extent that it affects the main claims and/or conclusions of the paper (regardless of whether the code and data are provided or not)?

Answer: [\[Yes\]](#)

Justification: The paper fully discloses all the information needed to reproduce the main experimental results.

Guidelines:

- The answer NA means that the paper does not include experiments.
- If the paper includes experiments, a No answer to this question will not be perceived well by the reviewers: Making the paper reproducible is important, regardless of whether the code and data are provided or not.
- If the contribution is a dataset and/or model, the authors should describe the steps taken to make their results reproducible or verifiable.
- Depending on the contribution, reproducibility can be accomplished in various ways. For example, if the contribution is a novel architecture, describing the architecture fully might suffice, or if the contribution is a specific model and empirical evaluation, it may be necessary to either make it possible for others to replicate the model with the same dataset, or provide access to the model. In general, releasing code and data is often one good way to accomplish this, but reproducibility can also be provided via detailed instructions for how to replicate the results, access to a hosted model (e.g., in the case of a large language model), releasing of a model checkpoint, or other means that are appropriate to the research performed.
- While NeurIPS does not require releasing code, the conference does require all submissions to provide some reasonable avenue for reproducibility, which may depend on the nature of the contribution. For example
 - (a) If the contribution is primarily a new algorithm, the paper should make it clear how to reproduce that algorithm.
 - (b) If the contribution is primarily a new model architecture, the paper should describe the architecture clearly and fully.
 - (c) If the contribution is a new model (e.g., a large language model), then there should either be a way to access this model for reproducing the results or a way to reproduce the model (e.g., with an open-source dataset or instructions for how to construct the dataset).
 - (d) We recognize that reproducibility may be tricky in some cases, in which case authors are welcome to describe the particular way they provide for reproducibility. In the case of closed-source models, it may be that access to the model is limited in some way (e.g., to registered users), but it should be possible for other researchers to have some path to reproducing or verifying the results.

5. Open access to data and code

Question: Does the paper provide open access to the data and code, with sufficient instructions to faithfully reproduce the main experimental results, as described in supplemental material?

Answer: [Yes]

Justification: The data and code will be released once prepared.

Guidelines:

- The answer NA means that paper does not include experiments requiring code.
- Please see the NeurIPS code and data submission guidelines (<https://nips.cc/public/guides/CodeSubmissionPolicy>) for more details.
- While we encourage the release of code and data, we understand that this might not be possible, so “No” is an acceptable answer. Papers cannot be rejected simply for not including code, unless this is central to the contribution (e.g., for a new open-source benchmark).
- The instructions should contain the exact command and environment needed to run to reproduce the results. See the NeurIPS code and data submission guidelines (<https://nips.cc/public/guides/CodeSubmissionPolicy>) for more details.
- The authors should provide instructions on data access and preparation, including how to access the raw data, preprocessed data, intermediate data, and generated data, etc.
- The authors should provide scripts to reproduce all experimental results for the new proposed method and baselines. If only a subset of experiments are reproducible, they should state which ones are omitted from the script and why.
- At submission time, to preserve anonymity, the authors should release anonymized versions (if applicable).
- Providing as much information as possible in supplemental material (appended to the paper) is recommended, but including URLs to data and code is permitted.

6. Experimental setting/details

Question: Does the paper specify all the training and test details (e.g., data splits, hyper-parameters, how they were chosen, type of optimizer, etc.) necessary to understand the results?

Answer: [Yes]

Justification: The paper provides details of implementation in Appendix F.

Guidelines:

- The answer NA means that the paper does not include experiments.
- The experimental setting should be presented in the core of the paper to a level of detail that is necessary to appreciate the results and make sense of them.
- The full details can be provided either with the code, in appendix, or as supplemental material.

7. Experiment statistical significance

Question: Does the paper report error bars suitably and correctly defined or other appropriate information about the statistical significance of the experiments?

Answer: [Yes]

Justification: We report the average results under five different random seeds and report the variance in Figure 5.

Guidelines:

- The answer NA means that the paper does not include experiments.
- The authors should answer "Yes" if the results are accompanied by error bars, confidence intervals, or statistical significance tests, at least for the experiments that support the main claims of the paper.
- The factors of variability that the error bars are capturing should be clearly stated (for example, train/test split, initialization, random drawing of some parameter, or overall run with given experimental conditions).
- The method for calculating the error bars should be explained (closed form formula, call to a library function, bootstrap, etc.)
- The assumptions made should be given (e.g., Normally distributed errors).

- It should be clear whether the error bar is the standard deviation or the standard error of the mean.
- It is OK to report 1-sigma error bars, but one should state it. The authors should preferably report a 2-sigma error bar than state that they have a 96% CI, if the hypothesis of Normality of errors is not verified.
- For asymmetric distributions, the authors should be careful not to show in tables or figures symmetric error bars that would yield results that are out of range (e.g. negative error rates).
- If error bars are reported in tables or plots, The authors should explain in the text how they were calculated and reference the corresponding figures or tables in the text.

8. Experiments compute resources

Question: For each experiment, does the paper provide sufficient information on the computer resources (type of compute workers, memory, time of execution) needed to reproduce the experiments?

Answer: [Yes]

Justification: The paper provide sufficient information on the computer resources.

Guidelines:

- The answer NA means that the paper does not include experiments.
- The paper should indicate the type of compute workers CPU or GPU, internal cluster, or cloud provider, including relevant memory and storage.
- The paper should provide the amount of compute required for each of the individual experimental runs as well as estimate the total compute.
- The paper should disclose whether the full research project required more compute than the experiments reported in the paper (e.g., preliminary or failed experiments that didn't make it into the paper).

9. Code of ethics

Question: Does the research conducted in the paper conform, in every respect, with the NeurIPS Code of Ethics <https://neurips.cc/public/EthicsGuidelines>?

Answer: [Yes]

Justification: The research conducted in the paper conform, in every respect, with the NeurIPS Code of Ethics.

Guidelines:

- The answer NA means that the authors have not reviewed the NeurIPS Code of Ethics.
- If the authors answer No, they should explain the special circumstances that require a deviation from the Code of Ethics.
- The authors should make sure to preserve anonymity (e.g., if there is a special consideration due to laws or regulations in their jurisdiction).

10. Broader impacts

Question: Does the paper discuss both potential positive societal impacts and negative societal impacts of the work performed?

Answer: [Yes]

Justification: The paper has discussed societal impacts in Appendix A.

Guidelines:

- The answer NA means that there is no societal impact of the work performed.
- If the authors answer NA or No, they should explain why their work has no societal impact or why the paper does not address societal impact.
- Examples of negative societal impacts include potential malicious or unintended uses (e.g., disinformation, generating fake profiles, surveillance), fairness considerations (e.g., deployment of technologies that could make decisions that unfairly impact specific groups), privacy considerations, and security considerations.

- The conference expects that many papers will be foundational research and not tied to particular applications, let alone deployments. However, if there is a direct path to any negative applications, the authors should point it out. For example, it is legitimate to point out that an improvement in the quality of generative models could be used to generate deepfakes for disinformation. On the other hand, it is not needed to point out that a generic algorithm for optimizing neural networks could enable people to train models that generate Deepfakes faster.
- The authors should consider possible harms that could arise when the technology is being used as intended and functioning correctly, harms that could arise when the technology is being used as intended but gives incorrect results, and harms following from (intentional or unintentional) misuse of the technology.
- If there are negative societal impacts, the authors could also discuss possible mitigation strategies (e.g., gated release of models, providing defenses in addition to attacks, mechanisms for monitoring misuse, mechanisms to monitor how a system learns from feedback over time, improving the efficiency and accessibility of ML).

11. Safeguards

Question: Does the paper describe safeguards that have been put in place for responsible release of data or models that have a high risk for misuse (e.g., pretrained language models, image generators, or scraped datasets)?

Answer: [NA] .

Justification: The paper poses no such risks.

Guidelines:

- The answer NA means that the paper poses no such risks.
- Released models that have a high risk for misuse or dual-use should be released with necessary safeguards to allow for controlled use of the model, for example by requiring that users adhere to usage guidelines or restrictions to access the model or implementing safety filters.
- Datasets that have been scraped from the Internet could pose safety risks. The authors should describe how they avoided releasing unsafe images.
- We recognize that providing effective safeguards is challenging, and many papers do not require this, but we encourage authors to take this into account and make a best faith effort.

12. Licenses for existing assets

Question: Are the creators or original owners of assets (e.g., code, data, models), used in the paper, properly credited and are the license and terms of use explicitly mentioned and properly respected?

Answer: [Yes]

Justification: We have cited the original paper that produced the code package and dataset.

Guidelines:

- The answer NA means that the paper does not use existing assets.
- The authors should cite the original paper that produced the code package or dataset.
- The authors should state which version of the asset is used and, if possible, include a URL.
- The name of the license (e.g., CC-BY 4.0) should be included for each asset.
- For scraped data from a particular source (e.g., website), the copyright and terms of service of that source should be provided.
- If assets are released, the license, copyright information, and terms of use in the package should be provided. For popular datasets, paperswithcode.com/datasets has curated licenses for some datasets. Their licensing guide can help determine the license of a dataset.
- For existing datasets that are re-packaged, both the original license and the license of the derived asset (if it has changed) should be provided.

- If this information is not available online, the authors are encouraged to reach out to the asset’s creators.

13. **New assets**

Question: Are new assets introduced in the paper well documented and is the documentation provided alongside the assets?

Answer: [\[Yes\]](#)

Justification: We communicate the details of the code as part of our submission via structured templates.

Guidelines:

- The answer NA means that the paper does not release new assets.
- Researchers should communicate the details of the dataset/code/model as part of their submissions via structured templates. This includes details about training, license, limitations, etc.
- The paper should discuss whether and how consent was obtained from people whose asset is used.
- At submission time, remember to anonymize your assets (if applicable). You can either create an anonymized URL or include an anonymized zip file.

14. **Crowdsourcing and research with human subjects**

Question: For crowdsourcing experiments and research with human subjects, does the paper include the full text of instructions given to participants and screenshots, if applicable, as well as details about compensation (if any)?

Answer: [\[NA\]](#)

Justification: The paper does not involve crowdsourcing and research with human subjects.

Guidelines:

- The answer NA means that the paper does not involve crowdsourcing nor research with human subjects.
- Including this information in the supplemental material is fine, but if the main contribution of the paper involves human subjects, then as much detail as possible should be included in the main paper.
- According to the NeurIPS Code of Ethics, workers involved in data collection, curation, or other labor should be paid at least the minimum wage in the country of the data collector.

15. **Institutional review board (IRB) approvals or equivalent for research with human subjects**

Question: Does the paper describe potential risks incurred by study participants, whether such risks were disclosed to the subjects, and whether Institutional Review Board (IRB) approvals (or an equivalent approval/review based on the requirements of your country or institution) were obtained?

Answer: [\[NA\]](#)

Justification: The paper does not involve crowdsourcing and research with human subjects.

Guidelines:

- The answer NA means that the paper does not involve crowdsourcing nor research with human subjects.
- Depending on the country in which research is conducted, IRB approval (or equivalent) may be required for any human subjects research. If you obtained IRB approval, you should clearly state this in the paper.
- We recognize that the procedures for this may vary significantly between institutions and locations, and we expect authors to adhere to the NeurIPS Code of Ethics and the guidelines for their institution.
- For initial submissions, do not include any information that would break anonymity (if applicable), such as the institution conducting the review.

16. Declaration of LLM usage

Question: Does the paper describe the usage of LLMs if it is an important, original, or non-standard component of the core methods in this research? Note that if the LLM is used only for writing, editing, or formatting purposes and does not impact the core methodology, scientific rigorousness, or originality of the research, declaration is not required.

Answer: [NA]

Justification: The core method development in this research does not involve LLMs as any important, original, or non-standard components.

Guidelines:

- The answer NA means that the core method development in this research does not involve LLMs as any important, original, or non-standard components.
- Please refer to our LLM policy (<https://neurips.cc/Conferences/2025/LLM>) for what should or should not be described.

A Social impacts

The proposed AI-generated image detection framework substantially mitigates societal risks stemming from the misuse of generative models. By advancing the capability to detect synthetic media, such as deepfakes, this work strengthens efforts to combat disinformation and enhances trust in digital media across critical domains, including journalism and legal evidence.

B Limitation

Limitation. **1)** Although the proposed orthogonal principle provides an approach for designing various types of functions and its validity is widely supported by extensive empirical studies, we have not provided formal proof of the convergence of the generalization risk within the context of generated image detection. Thus, our future work will focus on establishing the theoretical foundations of the generalization of our approach. **2)** Although we consider a threat model to verify the robustness of detectors, we have not provided an aggressive scenario where generative models are trained to minimize the inconsistency between f_1 and $f_2 = f_1 \circ h$. Thus, we will investigate the potential of integrating effective, robust, and efficient detection methods into the training process of generative models to make the generated images more realistic. **3)** Despite numerous empirical studies validating the effectiveness of the proposed ConV, the impact of scaling up the self-supervised model on the performance of detecting generated images remains to be explored since collecting a larger dataset and training an expanded self-supervised model are beyond the scope of this study. Moreover, future work is needed to explore how the performance of ConV will be affected if self-supervised models are trained on generated images. Finally, given the ongoing evolution of generative models, integrating advanced Domain Adaptation techniques (Yang et al., 2023) with ConV appears promising.

C Derivation for Inconsistency

Here, we give the detailed derivation of Eq. 4. We expand these two functions at $\mathbf{x} := \mathbf{x}_{\mathcal{M}}(\mathbf{x}_g)$ for a given generated image \mathbf{x}_g ,

$$f_1(\mathbf{x}_g) = f_1(\mathbf{x}) + \nabla f_1(\mathbf{x})^\top (\mathbf{x}_g - \mathbf{x}), \quad f_2(\mathbf{x}_g) = f_2(\mathbf{x}) + \nabla f_2(\mathbf{x})^\top (\mathbf{x}_g - \mathbf{x}), \quad (16)$$

where we neglect the higher-order approximation error.

The inconsistency between generated images can be formalized by,

$$\delta(\mathbf{x}_g) = |f_1(\mathbf{x}) - f_2(\mathbf{x}) + (\nabla f_1(\mathbf{x}) - \nabla f_2(\mathbf{x}))^\top (\mathbf{x}_g - \mathbf{x})| = |(\nabla f_1(\mathbf{x}) - \nabla f_2(\mathbf{x}))^\top (\mathbf{x}_g - \mathbf{x})|, \quad (17)$$

where the equation holds because of $\delta(\mathbf{x}) = f_1(\mathbf{x}) - f_2(\mathbf{x}) = 0$. Then, we have

$$\delta(\mathbf{x}_g) = |(\nabla f_1(\mathbf{x}) - \nabla f_2(\mathbf{x}))^\top (\mathbf{x}_g - \mathbf{x})| \geq \|\nabla f_1(\mathbf{x})^\top (\mathbf{x}_g - \mathbf{x})\| - \|\nabla f_2(\mathbf{x})^\top (\mathbf{x}_g - \mathbf{x})\|. \quad (18)$$

D SOFTWARE AND HARDWARE

We use python 3.8.16 and Pytorch 1.12.1, and several NVIDIA GeForce RTX-3090 GPU and NVIDIA GeForce RTX-4090 GPU.

E Details of transformations

We follow the data augmentation strategy used when training DINOv2 with a combination of HorizontalFlip, ColorJitter, and GaussianBlur. For ColorJitter, brightness, contrast, saturation, and hue are randomly adjusted with a factor in the ranges of [0.88,1.12],[0.88,1.12],[0.94,1.06], and [0.97,1.03], respectively. For GaussianBlur, the kernel size is set to 9×9 , and the variance is randomly selected in [0.7,1].

F Implementation Details

To maintain detection efficiency, we set $n = 20$ in our experiments. For F-ConV, we train a RealNVP (Dinh et al., 2017) on the top of DINOv2 ViT-L/14, which consists of 2 coupling blocks

Table 3: AI-generated image detection performance on ImageNet.

Methods	ADM		ADMG		LDM		DiT		BigGAN		GigaGAN		StyleGAN XL		RQ-Transformer		Mask GIT		Average	
	AUROC	AP	AUROC	AP	AUROC	AP	AUROC	AP	AUROC	AP	AUROC	AP	AUROC	AP	AUROC	AP	AUROC	AP	AUROC (↑)	AP (↑)
Random rotation (-90-90 degrees)	74.43	75.23	67.44	66.45	65.60	65.12	65.47	65.71	75.20	76.89	71.72	74.41	74.66	77.13	76.36	77.62	71.21	72.95	71.34	72.39
Random rotation (-45-45 degrees)	79.91	79.12	71.61	68.80	69.65	66.87	70.03	68.12	82.11	81.95	79.21	79.65	83.09	83.58	82.79	82.03	77.91	77.54	77.37	76.41

with fully connected networks as internal functions. The model is optimized using the AdamW optimizer with a learning rate of 1×10^{-5} , $\beta_1 = 0.9$, $\beta_2 = 0.99$, and a weight decay of 0.01. Following CNNspot (Wang et al., 2020), data augmentation techniques, including JPEG compression and Gaussian blur, are applied to enhance model robustness. For the ImageNet and LSUN-Bedroom benchmarks, the ProGAN dataset is used as the training set. For the GenImage benchmark, the SDv1.4 dataset is employed as trainind set and the SDv2 dataset serves as the training set for the DRCT-2M benchmark. During testing, to ensure unbiased classification accuracy and mitigate biases from manually selected thresholds, we follow (Ojha et al., 2023) by automatically determining the optimal threshold. This threshold is selected to maximize the separation between natural and synthetic images based on their classification scores. An alternative approach involves optimizing the threshold on a small validation set. This method’s performance is sensitive to the validation set’s characteristics, such as its size and distributional representativeness. However, in real-world applications, the methods for determining thresholds may vary. For instance, to prioritize the detection of generated images, administrators may set a higher threshold, classifying only samples with similarity scores approaching 1 as natural images. This is consistent with the motivation of leveraging AUROC and AP as the main metric for evaluation.

G Details of Datasets

IMAGENET. The natural images and generated images can be obtained at <https://github.com/layer6ai-labs/dgm-eval>. The images are provided by (Stein et al., 2023). The resolution of natural images and generated images are 256×256 . The generated images include: ADM, ADMG, BigGAN, DiT-XL-2, GigaGAN, LDM, StyleGAN-XL, RQ-Transformer, Mask-GIT

LSUN-BEDROOM. The natural images and generated images can be obtained at <https://github.com/layer6ai-labs/dgm-eval>. The images are provided by (Stein et al., 2023). The resolution of natural images and generated images are 256×256 . We crop the image randomly to 224×224 resolution. The generated images include: ADM, DDPM, iDDPM, StyleGAN, Diffusion-Projected GAN, Projected GAN, Unleashing Transformers.

GenImage. The natural images and generated images can be obtained at <https://github.com/GenImage-Dataset/GenImage>. The images are provided by (Zhu et al., 2023b). The natural images come from ImageNet, and different images have different resolutions. The generative model includes Midjourney, SD V1.4, SD V1.5, ADM, GLIDE, Wukong, VQDM, and BigGAN.

DRCT-2M. The natural images of DRCT-2M come from CoCo and can be obtained from <https://cocodataset.org/#download>. AI-generated images of DRCT-2M can be obtained from <https://modelscope.cn/datasets/BokingChen/DRCT-2M/files>, which are provided by (Chen et al., 2024). The generative model includes LDM, SDv1.4, SDv1.5, SDv2, SDXL, SDXL-Refiner, SD-Turbo, SDXL-Turbo, LCM-SDv1.5, LCM-SDXL, SDv1-Ctrl, SDv2-Ctrl, SDXL-Ctrl, SDv1-DR, SDv2-DR, SDXL-DR.

H Results of using other data transformations.

In our experiments, we leverage data augmentations used in the training phase, including geometric augmentations, color jitter, and Gaussian blur. We further conduct comparison experiments using data augmentations which is not used during training, such as random rotation. The experiments are conducted on the ImageNet benchmark. As shown Table 3, using data transformations not seen during training does not result in

Table 4: Ablation studies on F-ConV.

Method	AUROC	AP
F-ConV	93.77	93.38
w/o Shaping Loss	89.17	87.89
w/o Consistency Loss	92.54	91.66

Table 6: AI-generated image detection performance on ImageNet.

Methods	ADM		ADMG		LDM		DIT		BigGAN		GigaGAN		StyleGAN XL		RQ-Transformer		Mask GIT		Average	
	AUROC	AP	AUROC	AP	AUROC	AP	AUROC	AP	AUROC	AP	AUROC	AP	AUROC	AP	AUROC	AP	AUROC	AP	AUROC (↑)	AP (↑)
Training-based Methods																				
CNNspot	62.25	63.13	63.28	62.27	63.16	64.81	62.85	61.16	85.71	84.93	74.85	71.45	68.41	68.67	61.83	62.91	60.98	61.69	67.04	66.78
Ojha	83.37	82.95	79.60	78.15	80.35	79.71	82.93	81.72	93.07	92.77	87.45	84.88	85.36	83.15	85.19	84.22	90.82	90.71	85.35	84.25
DIRE	51.82	50.29	53.14	52.96	52.83	51.84	54.67	55.10	51.62	50.83	50.70	50.27	50.95	51.36	55.95	54.83	52.58	52.10	52.70	52.18
NPR	85.68	80.86	84.34	79.79	91.98	86.96	86.15	81.26	89.73	84.46	82.21	78.20	84.13	78.73	80.21	73.21	89.61	84.15	86.00	80.84
Training-free Methods																				
AEROBLADA	55.61	54.26	61.57	56.58	62.67	60.93	85.88	87.71	44.36	45.66	47.39	48.14	47.28	48.54	67.05	67.69	48.05	48.75	57.87	57.85
ConV-DINOv2	88.89	86.60	82.46	79.83	78.94	75.88	75.25	70.11	92.83	92.05	91.89	90.93	92.15	91.82	93.02	91.26	88.79	87.88	87.13	85.15
ConV-CLIP:unimodal	76.64	76.52	69.36	68.86	70.29	69.73	70.03	69.73	76.59	79.27	72.97	73.05	70.82	70.35	77.27	77.49	72.95	73.20	72.99	72.98
ConV-CLIP:multimodal	80.76	79.77	72.31	71.21	72.03	71.22	72.73	72.12	80.73	76.60	79.59	77.47	77.46	75.17	80.83	78.86	74.34	70.45	76.75	74.76

good detection performance. Since the rotations were not used for data augmentation during training, using them to perform ConV during testing could not achieve good detection performance.

I Ablation studies on the transformation functions

As shown in Table 5, we conduct additional ablation studies evaluating the effectiveness of various transformation functions. The results indicate that the three transformations examined exhibit comparable performance.

J Ablation studies on F-ConV

As shown in Table 4, we perform ablation experiments on the two loss functions used in F-ConV. The results validate the effectiveness of our approach.

K Analysis of Failure Cases

As shown in Figure 9, we demonstrate some failure cases of ConV. We compute the original features and transformed features on highly realistic generated images. It can be observed that the features of these highly realistic generated images also remain virtually unchanged, leading the model to incorrectly classify them as natural images.

L Results on CLIP

In our paper, we use DINOv2 for all of our experiments. We further use CLIP for comparison experiments. We note that the authors only used randomly crop as data augmentation when training CLIP. Therefore, when implementing ConV with CLIP, we also only use random crop. As shown in Table 6, using CLIP to implement ConV does not achieve good performance. We speculate that this difference comes from the training methodology. CLIP learns features using image captions as supervision, which may make the features more focused on semantic information, whereas DINOv2 learns features only from images, which makes it more focused on the images themselves, and thus better able to capture the subtle differences between the natural image and the generated image. In addition to this, the fact that CLIP only uses random crop as data augmentation may also contribute to the poor performance of ConV.

The results show that our method performs relatively worse when using CLIP. To overcome this limitation, we revisit our methodology, i.e., verifying the consistency between outputs of two functions.

As shown in Eq. (13), we derive the cosine similarity metric between image features from a self-supervised learning objective function. However, CLIP employs a different objective function, namely, calculating the similarity between text and image features. Thus, the proposed cosine similarity

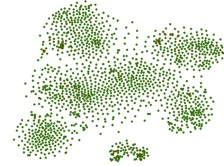


Figure 9: ConV fails on highly realistic generated images.

between image features may not be a good realization of these two functions' output, limiting the generalization capability for generated image detection. We conjecture the difference between the projection of the visual features of the original image and the visual features of the transformed image on their corresponding text features would be a good metric. The reason is as follows: The function to calculate the similarity between text and image features can be regarded as a function. Thus, we should calculate the difference in inter-modality similarity rather than the similarity between original and transformed images. To verify the point, we conduct experiments using the corrected realization of f_1 and f_2 , i.e., a corrected metric to verify the consistency. The results below show that the modified approach outperforms the original metric.

These results show that using the modified metric for detection greatly improves the performance of CLIP-based methods model, achieving performance comparable with Dinov2-based methods. Hence, we believe our work provides a novel approach to calculating the difference between two functions without focusing on the differences in similarities between two image features.

M Results on GenImage, DRCT-2M and LSUN-BEDROOM

As shown in Table 7, Table 9 and Table 8, our method achieves good performance on GenImage, DRCT-2M and LSUN-BEDROOM, confirming the robustness of the proposed method.

Table 7: AI-generated image detection performance (ACC, %) on GenImage.

Methods	Models								
	Midjourney	SD V1.4	SD V1.5	ADM	GLIDE	Wukong	VQDM	BigGAN	Average
Training Methods									
ResNet-50	54.9	99.9	99.7	53.5	61.9	98.2	56.6	52.0	72.1
DeiT-S	55.6	99.9	99.8	49.8	58.1	98.9	56.9	53.5	71.6
Swin-T	62.1	99.9	99.8	49.8	67.6	99.1	62.3	57.6	74.8
CNNspot	52.8	96.3	95.9	50.1	39.8	78.6	53.4	46.8	64.2
Spec	52.0	99.4	99.2	49.7	49.8	94.8	55.6	49.8	68.8
F3Net	50.1	99.9	99.9	49.9	50.00	99.9	49.9	49.9	68.7
GramNet	54.2	99.2	99.1	50.3	54.6	98.9	50.8	51.7	69.9
DIRE	60.2	99.9	99.8	50.9	55.0	99.2	50.1	50.2	70.7
Ojha	73.2	84.2	84.0	55.2	76.9	75.6	56.9	80.3	73.3
NPR	81.0	98.2	97.9	76.9	89.8	96.9	84.1	84.2	88.6
FatFormer	92.7	100.0	99.9	75.9	88.0	99.9	98.8	55.8	88.9
GenDet	89.6	96.1	96.1	58.0	78.4	92.8	66.5	75.0	81.6
DRCT	91.5	95.0	94.4	79.4	89.1	94.6	90.0	81.6	89.4
F-Conv	89.3	98.8	98.5	74.9	89.3	95.6	86.7	87.6	90.1
Training-free Methods									
AEROBLADE	80.3	87.5	86.8	67.2	81.5	83.7	51.1	52.5	73.83
ConV	85.13	76.74	74.53	73.80	72.97	80.00	87.57	89.94	80.08

Table 8: Detection performance (%) on LSUN-Bedroom.

Methods	Models														Average	
	ADM		DDPM		iDDPM		Diffusion GAN		Projected GAN		StyleGAN		Unleashing Transformer			
	AUROC	AP	AUROC	AP	AUROC	AP	AUROC	AP	AUROC	AP	AUROC	AP	AUROC	AP	AUROC (↑)	AP (↑)
CNNspot	64.83	64.24	79.04	80.58	76.95	76.28	88.45	87.19	90.80	89.94	95.17	94.94	93.42	93.11	84.09	83.75
Ojha	71.26	70.95	79.26	78.27	74.80	73.46	84.56	82.91	82.00	78.42	81.22	78.08	83.58	83.48	79.53	77.94
DIRE	57.19	56.85	61.91	61.35	59.82	58.29	53.18	53.48	55.35	54.93	57.66	56.90	67.92	68.33	59.00	58.59
NPR	75.43	72.60	91.42	90.89	89.49	88.25	76.17	74.19	75.07	74.59	68.82	63.53	84.39	83.67	80.11	78.25
F-ConV	76.59	74.40	93.53	92.16	88.90	86.85	98.10	98.03	97.93	97.81	91.63	90.16	97.31	96.91	92.00	90.91
AEROBLADA	57.05	58.37	61.57	61.49	59.82	61.06	47.12	48.25	45.98	46.15	45.63	47.06	59.71	57.34	53.85	54.25
ConV	73.71	71.52	87.74	86.59	82.96	81.79	93.79	93.87	94.73	94.74	84.10	82.35	93.75	93.51	87.25	86.34

Table 9: AI-generated image detection performance (ACC, %) on DRCT-2M.

Method	SD Variants					Turbo Variants		LCM Variants			ControlNet Variants			DR Variants			Avg.
	LDM	SDv1.4	SDv1.5	SDv2	SDXL	SDXL-Refiner	SD-Turbo	SDXL-Turbo	LCM-SDv1.5	LCM-SDXL	SDv1-Ctrl	SDv2-Ctrl	SDXL-Ctrl	SDv1-DR	SDv2-DR	SDXL-DR	
CNNspot	99.87	99.91	99.90	97.63	66.25	86.55	86.15	72.42	98.26	61.72	97.96	85.89	82.94	60.93	51.41	50.28	81.12
F3Net	99.85	99.78	99.79	88.60	55.85	87.37	63.29	63.66	97.39	54.98	97.98	72.39	81.99	65.42	50.39	50.27	71.13
CLIP/RN50	99.00	99.99	99.96	94.61	62.08	91.43	84.40	64.40	98.97	57.43	99.74	80.69	82.03	65.83	50.67	50.47	80.05
GramNet	99.40	99.01	98.84	95.30	62.63	80.68	71.19	69.32	93.05	57.02	89.97	75.55	82.68	51.23	50.01	50.08	76.62
De-fake	92.1	95.53	99.51	89.65	64.02	69.24	92.00	93.93	99.13	70.89	58.98	62.34	66.66	50.12	50.16	50.00	75.52
Conv-B	99.97	100.0	99.97	95.84	64.44	82.00	60.75	99.27	99.27	62.33	99.80	83.40	73.28	61.65	51.79	50.41	79.11
Ojha	98.30	96.22	96.33	93.83	91.01	93.91	86.38	85.92	90.44	89.99	90.41	81.06	89.06	51.96	51.03	50.46	83.46
DIRE	54.62	75.89	76.04	99.87	59.90	93.08	97.55	87.29	72.53	67.85	99.69	64.40	64.40	49.96	52.48	49.92	72.55
DRCT	94.45	94.35	94.24	95.05	96.41	95.38	94.81	94.48	91.66	95.54	93.86	93.50	93.54	84.34	83.20	67.61	91.35
FatFormer	96.52	95.31	93.27	91.99	92.87	91.78	88.15	87.48	92.82	91.76	90.28	86.99	88.19	65.92	60.15	55.13	85.53
ConV	88.12	74.75	73.17	79.13	82.10	89.53	78.25	77.92	77.15	86.37	77.67	77.85	86.73	62.79	60.18	57.83	76.84
F-ConV	99.07	98.38	98.84	99.05	98.75	99.50	98.29	97.66	98.58	98.99	98.56	98.01	97.95	69.74	65.87	64.88	92.63

Table 10: generated image detection performance with different pre-trained models.

Methods	MoCo		SwAV		Models DINO		CLIP		DINOv2	
	AUROC	AP	AUROC	AP	AUROC	AP	AUROC	AP	AUROC	AP
ConV	68.43	67.65	74.71	73.48	71.91	69.46	72.99	72.98	87.13	85.15

N Result on more pre-trained models

Besides CLIP, we conduct experiments using the MoCo (He et al., 2020), SwAV (Caron et al., 2020), and DINO (Caron et al., 2021). The results are reported in Table 10. These results show that our method can be applied to various backbones.

Table 11: Experimental results on Flux.

Method	AUROC	AP
ConV	87.38	89.19
F-ConV	90.18	90.65

O Experimental results on Flux

To further assess the generalization capabilities of ConV, we evaluate its performance against the advanced FLUX.1 [dev] generative model (Batifol et al., 2025), which was not encountered during training. For this analysis, a new benchmark dataset is constructed, comprising 6,000 images generated by FLUX.1 [dev] and an equal number of natural images sampled from ImageNet. As presented in Table 11, ConV demonstrates robust performance on this unseen model, underscoring the strong cross-model generalizability of our approach.

P Comparison with Linear Classifiers

To further demonstrate the effectiveness of our approach, we additionally train a binary classifier on the DINOv2 embeddings using the same training set. As shown in Table 12, the performance of the directly trained binary classifier falls short of that achieved by F-ConV, highlighting the advantage of our manifold-based approach.

Table 12: Comparison with Linear Classifiers.

Method	AUROC	AP
ConV	87.38	89.19
F-ConV	90.18	90.65
Linear classification	87.83	86.49